Известия вузов России. Радиоэлектроника. 2022. Т. 25, № 5. С. 56–66
Journal of the Russian Universities. Radioelectronics. 2022, vol. 25, no. 5, pp. 56–66

Radar and Navigation

UDC 621.391 Original article

https://doi.org/10.32603/1993-8985-2022-25-5-56-66

Research and Design of an X-Band UHF Power Amplifier

Xuan Luong Nguyen[1], Thanh Thuy Dang Thi[1],
Phung Bao Nguyen[2]✉, Van Bac Nguyen[2]

[1]VNU University of Science, Hanoi, Vietnam

[2]Le Quy Don Technical University, Hanoi, Vietnam

✉nguyenphungbao@lqdtu.edu.vn

Abstract

Introduction. A method for designing power amplifiers for use in the transmitting channels of X-band transceiver modules is investigated. The design process was aimed at optimizing the relationship between the basic amplifier characteristics, including the operating frequency band, output power level, output linearity, high harmonics suppression, etc.

Aim. Investigation of a method for designing an X-band UHF power amplifier, which is capable of optimizing the relationship between its main characteristics.

Materials and methods. Theoretical calculations were combined with experimental studies into the design of a UHF power amplifier. The stages of the design process are described in detail, including major ideas, principal circuits, and strip circuits. Evaluations were conducted using the Keysight ADS high frequency circuit simulation tool.

Results. A method for designing X-band UHF power amplifiers on the basis of a close combination of theory, simulation, and experimental adjustment was described in detail.

Conclusion. A prototype of an X-band PA was developed; an approach to developing a methodology for manufacturing, measuring, and testing X-band PAs is described.

Keywords: ultra-high-frequency power amplifier (UHF PA), power amplifier element (PA element), power added efficiency (PAE)

For citation: Xuan Luong Nguyen, Thanh Thuy Dang Thi, Phung Bao Nguyen, Van Bac Nguyen. Research and Design of an X-Band UHF Power Amplifier. Journal of the Russian Universities. Radioelectronics. 2022, vol. 25, no. 5, pp. 56–66. doi: 10.32603/1993-8985-2022-25-5-56-66

Conflict of interest. The authors declare no conflicts of interest.

Acknowledgements. The paper is part of the scientific and technological project "Research and design of multifunctional radio navigation systems X-band" chaired by the Research Institute of Radio Positioning Systems SRV.

Submitted 05.07.2022; accepted 09.08.2022; published online 29.11.2022

Introduction. Ultra-high-frequency (UHF) power amplifiers (PA) are indispensable components in the transmitting channels of modern radio engineering systems, such as multi-function radio navigation systems based on digital phased antenna arrays [1, 16]. Success in creating high-performance power amplifiers (WPAs) with a sufficiently wide frequency band is determined by a combination of calculation methods, optimal circuitry, rational design, and advanced active device technology. Moreover, these components are closely intertwined and cannot be considered in isolation. The quality of PAs is determined by their basic characteristics, including the operating frequency band, output power level, gain, power added efficiency (PAE), nonlinear distortion (ND), etc. [2, 3]

Numerous works have described approaches to the design of UHF PAs capable of simultaneously ensuring (or weighted priority) the above characteristics [2–4, 8–11, 14]. Some typical approaches include those based on:

– application of some special mods (or their combinations) of the amplifier element in order to ensure the selected PA characteristics [4–9, 11];

– a response to each independent characteristic to be developed and ensured by the corresponding in-dependent circuit [12];

– a general analysis of the theory and methodology, as well as technical requirements of systems capable of establishing the relationship between the UHF PA characteristics. This approach is aimed at providing solutions to ensure the maximum objective functionality of the entire system [10].

According to [3], the former two approaches provide relatively simple solutions to the requirements set for UHF PAs. This particularly concerns the second approach. However, such products are frequently characterized by a complex design, large size, high production costs, and the difficulty of technical maintenance.

In this work, rather than proposing a new approach, we carry out an in-depth study and specification of a design method based on the third approach, which can be conventionally referred to as a design method based on theoretical calculations combined with experimental adjustments. The essence of this approach is illustrated by an example of UHF PA design in the X-band.

The paper is organized as follows. First, we present an approach to designing an X-band UHF PA that optimizes the ratio between its important parameters. Then we describe the design process and investigate the developed system. Finally, some conclusions are drawn.

The process of designing an X-band UHF PA.

Input specifications. The input specifications for PA design are presented in Tab. 1.

Tab. 1. Input specifications for design PA

№	Input specification	Value
1	Frequency range, GHz	8.9…9.8
2	Output power at compression point 1dB P_{1dB}, dBm	36
3	Power gain, dB	11
4	PAE, %	~40

The design process includes the following steps: selection of an amplifier element; circuit selection and setting the static operating point; estimation of load/source impedances; impedance matching circuit design; voltage divider circuit design, etc. The basic expressions for theoretical calculations can be found in the design materials published as recommendations. Care should be taken to ensure optimal matching of the main characteristics of the amplifier based on not only theoretical statements, but also experimental adjustments.

Selection of the amplifier element.

1. Based on the input specifications, we preliminarily selected an MMIC transistor, which is a TGF2977-SM transistor based on a high electronic mobility technology (HEMT) manufactured by the Quorvo company as a UHF amplifier element with a broadband. The main parameters of TGF2977-SM are presented in Tab. 2 [17, 18].

Tab. 2. The main parameters of TGF2977-SM

№	Input specification	Value
1	Frequency range, GHz	DC ÷ 12
2	Output power at compression point 3 dB P_{3dB}, W	~5W
3	Linear power gain, dB	$13\big\vert_{f=9.4Gz}$
4	PAE at compression point 3 dB P_{3dB}, %	≥ 50
5	Operating Voltage, V	32
6	Capable of working in both pulsed and continuous mode	

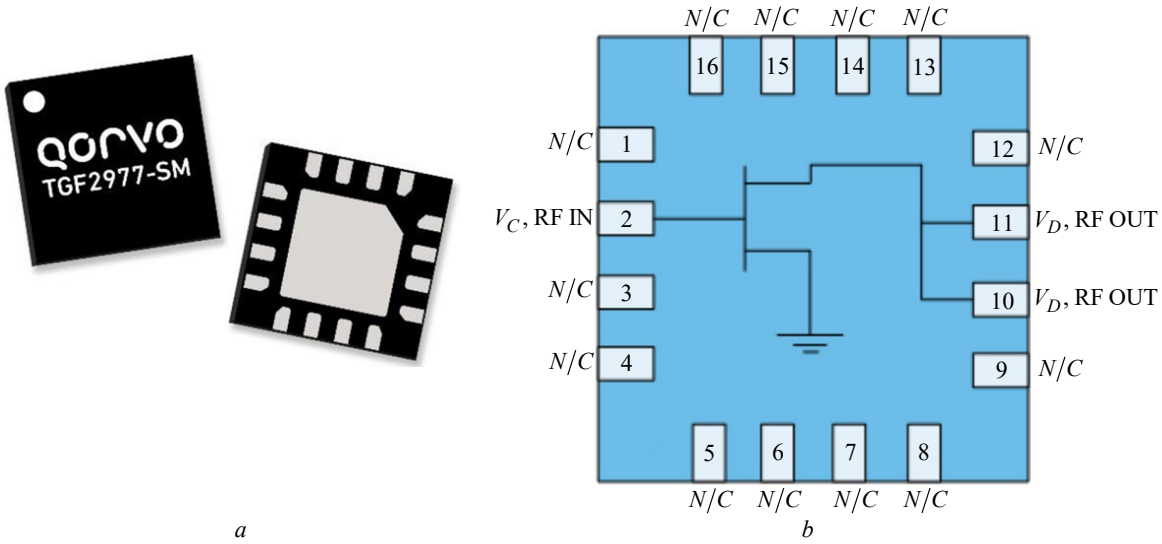

Fig. 1. Actual representation (*a*) and the QFN functional pin assignment (*b*) of TGF2977-SM

The accuracy of the selected transistor model was verified using the Keysight ADS high-frequency circuit simulation tool [19, 20].

Fig. 1 shows the actual representation (*a*) and the QFN-type functional pin assignment (*b*) of TGF2977-SM.

2. According to [18], the model for the TGF2977-SM element, referred to as HMT-QOR-TGF2977-SM-01, is a large-signal non-linear model whose parameters are extracted from a large-signal model. This data is mapped against scatter matrix measurements $[S]$ and load data of a large Load and Pull signal in the range 6…11 GHz. Fig. 2, *a* shows the HMT-QOR-TGF2977-SM-01 reference plane. Fig. 2, *b* demonstrates the element pins (after packaging) for data output (by Keysight ADS high-frequency circuit simulation tool).

3. Validation of the large signal model is of particular importance in UHF PA design, since this model allows the characteristics of the amplifier to be accurately determined. This process is carried out using load and source pull measurements [19]. The validation process is performed under the condition: $f = 9$ GHz; voltage drain-source $V_{\text{DS}} = 32\,\text{V}$; current flowing through drain-source $I_{\text{DS}} = 25\,\text{mA}$; the characteristic impedance of $15\,\Omega$ and room temperature 25 °C. The output power (at the compression point of 3 dB) and PAE for the HMT-QOR-TGF2977-SM-01 model and for the actual component TGF2977-SM are shown in Fig. 3.

The sets of source and load impedance values used to perform simulations based on the model and actual measurements are as follows:

$$Z_S = 27.849 - j^* 42.543;$$

$$Z_{S_2} = 31.385 + j^* 22.690;$$

$$Z_{S_3} = 10.806 + j^* 0.743;$$

$$Z_{L_2} = 15.190 + j^* 11.058;$$

$$Z_{L_3} = 10.421 + j^* 3.104.$$

Fig. 2. Reference plane (*a*) and pins for measurements (after packaging) (*b*) of HMT-QOR-TGF2977

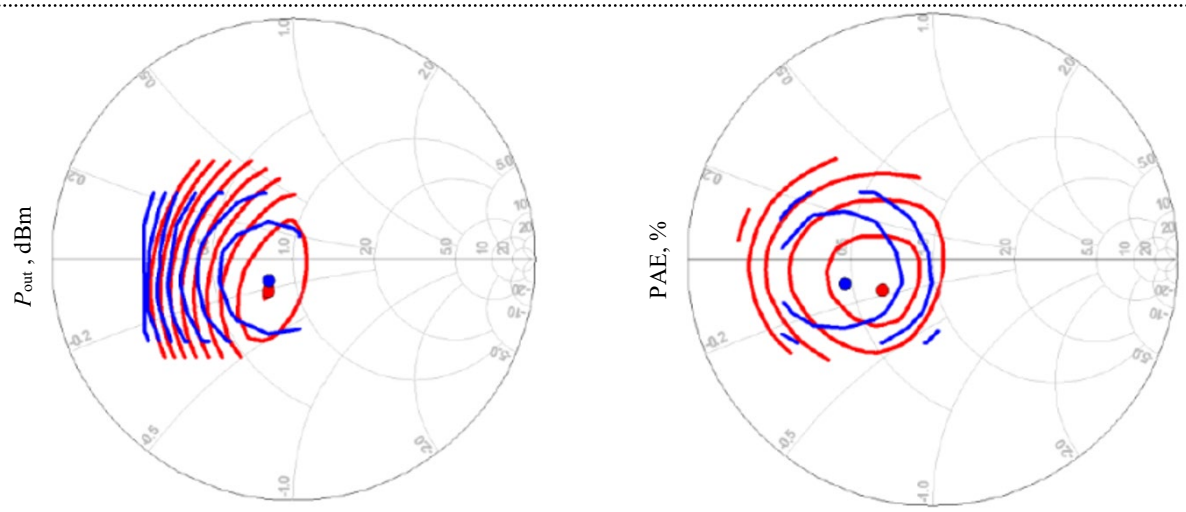

Fig. 3. Output power (at the compression point of 3 dB) and PAE results for the model (red) and for the actual element (blue)

Tab. 3. The optimal impedance of the model and of the real PA element at the f_0

Types	Optimum impedance for power, Ω	Maximum capacity, dBm	Optimum impedance for PAE, Ω	PAE_{max}, %
Model	$11.5 - j3.3$	37.8	$9.5 - j2.8$	52.3
Real PA	$12 - j2.3$	36.9	$6.9 - j1.8$	51.4

The data from Fig. 3 is used to determine impedances at f_0 of the model and actual PA element (component) as shown in Tab. 3.

Circuit selection and setting of the static operating point.

1. In order to simplify the design and to ease measurement and adjustment procedures when scaling the production process, we selected the circuit diagram of a single amplifier based on the TGF2977-SM transistor with a common source (CS) to provide the gain ratio and output power.

2. The selection and setting of the operating point for the UHF PA circuit is usually carried out based on the characteristics of components provided by the manufacturer. However, for the majority of new generation components, manufactures determine the optimal mode of their operation, rather than statistical characteristics. Thus, experimental measurements can be carried out based on the analysis of calculation and simulation results. Following the recommendations of the manufacturer, the setup procedure for TGF2977-SM in the AB mode is as follows: set up $V_{GS} = 4$ V; set up the current limit of $I_{DS} \sim 30$ mA; power supply $V_{DS} = 32$ V; make adjustments slowly to $I_{DS} \to 25$ mA; set up the pulse current limit of $I_{PDS} \sim 500$ mA.

Estimation of load/source impedances. An estimation of optimal source and load impedance values is performed separately by the source/load pull technique.

1. The load impedance is implemented by the load-pull technique in the ADS as shown in Fig. 4, *a*. The PA is designed considering the requirement of high performance. Therefore, it is necessary to estimate impedance at the f_0 frequency and at adjacent frequencies in the operating frequency range of the system. At 2nd and higher harmonics, impedance estimation is aimed at reducing the power loss across them. However, according to [2], when the PA element is set to the AB mod, the power loss at the 2nd harmonic is much larger than that of the other higher harmonics. Therefore, the determination of the load impedance at harmonics higher than the 2nd order can be omitted. However, in order to ensure a uniform quality during mass production and its adjustment, we added a pseudo short circuit for the 3rd harmonic in the output impedance matching circuit. In Fig. 4, *b*, lines show the level of output power and PAE for the diagram presented in Fig. 4, *a*. It can be seen from Fig. 4, *b* that the optimal load impedances at the center and neighborhood frequencies for the

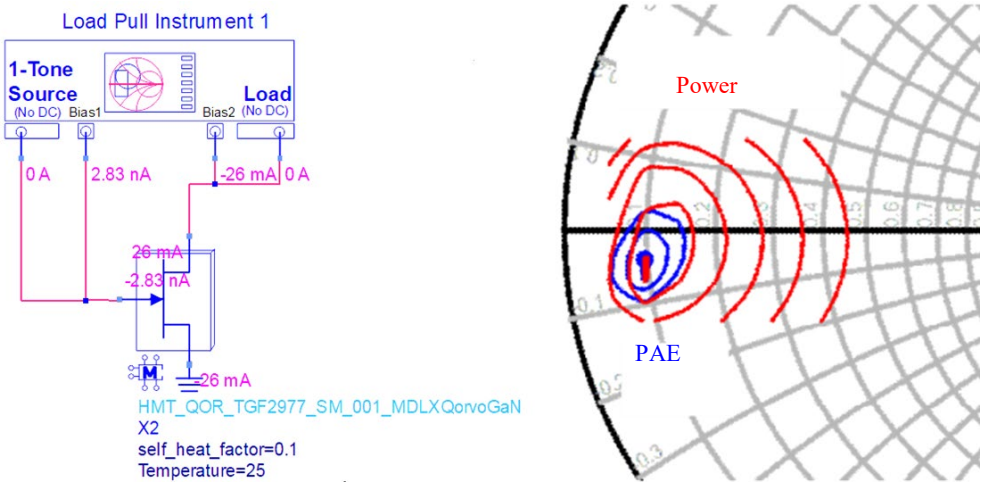

a *b*

Fig. 4. Load-pull simulation diagram in ADS (*a*) and the level of output power and PAE in the Smith diagram (*b*)

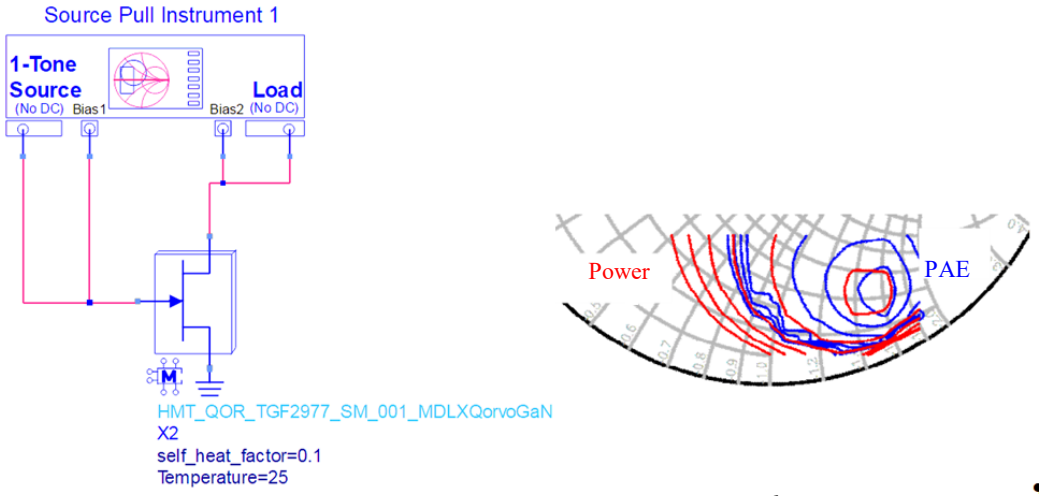

a *b*

Fig. 5. Source-pull simulation diagram in ADS (*a*) and the level of output power and PAE in the Smith diagram (*b*)

output power level and PAE are nearly identical at $Z_{L,f_0} \sim (9.6 - j4.1)\Omega$.

2. The source impedance was determined for the maximum value of PAE. In terms of the model, the source impedance is a complex conjugate of the input impedance of the PA element, estimated such that the reflected power loss at its input is minimized. The source impedance was optimized using the source pull technique as shown in Fig. 5, *a*. Fig. 5, *b* presents the contour lines of the output power and PAE. Since the output power level is determined as the target parameter, the optimal source impedance is selected at the maximum power of $Z_{S,f_0} \sim (28 - j96)\Omega$.

3. The determination of impedance values for high harmonics is carried out both at the source and load sides using the load-source pull technique. Fig. 6 presents the results of estimating the source and load impedance at the 2nd and 3rd harmonics.

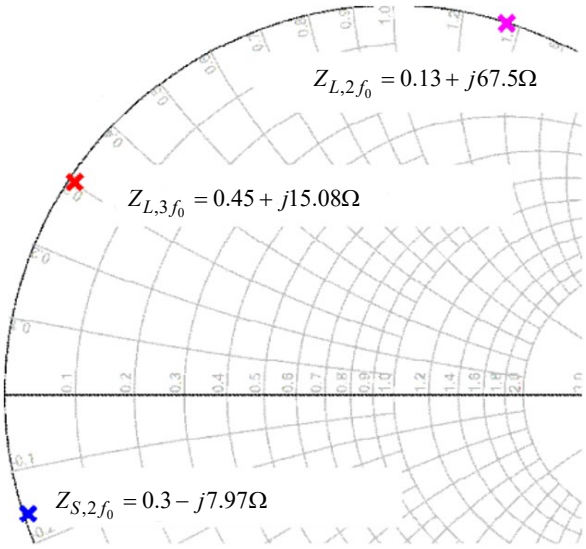

Fig. 6. Estimation results of the source and load impedance at the 2nd $Z_{S,2f_0}$ and 3rd harmonics $Z_{L,2f_0}, Z_{L,3f_0}$

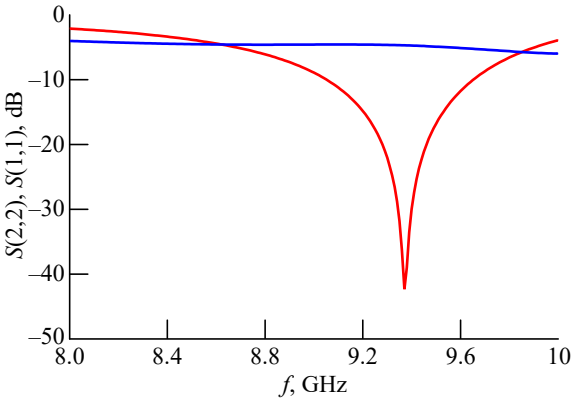

Fig. 7. Input (red) and output (blue) reverse loss characteristics of an ideal PA

Since these values fall into the boundary region of the Smith diagram, then, according to [13, 14], the phase difference between the instantaneous value of the current and the voltage will vary within the limits $\pm 90°$. As a result, the power loss at higher harmonics will be suppressed.

To further confirm that optimal source/load impedances match, the input/output reverse loss of the PA requires verification. Fig. 7 presents the results of determining the input (red) and output (green) characteristics of the reverse loss of an ideal PA.

Design of an impedance matching circuit. Impedance matching circuits are used to convert impedances into optimal source and load impedances in order to ensure minimal losses.

1. Fig. 8 shows the strip circuit (*a*) and the layout circuit (*b*) of the input impedance matching circuit.

At the strip circuit level (Fig. 8, *a*), the ideal paths will be converted to strip paths on the Rogers high frequency material RO4003C, for which the layout of the input impedance matching circuit is shown in Fig. 8, *b*. According to [2, 14, 15], to evaluate the quality of the input impedance matching circuit, the insertion loss characteristic of the following form can be used

$$\mathrm{IL} = 10\lg\left(\frac{1-|S_{11}|^2}{|S_{21}|^2}\right).$$

In this case, based on the measured results of S_{11}, S_{21} and the above expression, the obtained $\mathrm{IL} \sim 0.31\ldots0.28\ \mathrm{dB}\big|_{f=9\ldots11\ \mathrm{GHz}}$ is acceptable for the X band design.

2. Fig. 9 shows the strip circuit (*a*) and the layout circuit (*b*) of the output impedance matching circuit.

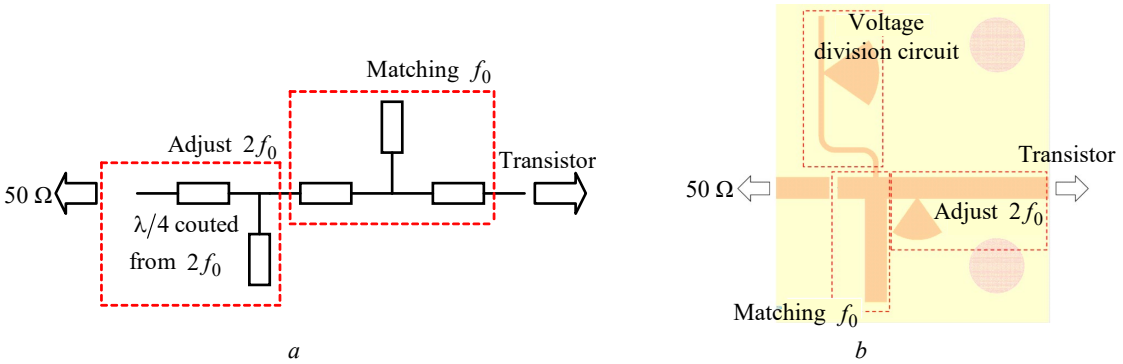

Fig. 8. Strip circuit of the input impedance matching at the ideal level (*a*) and layout circuit (*b*)

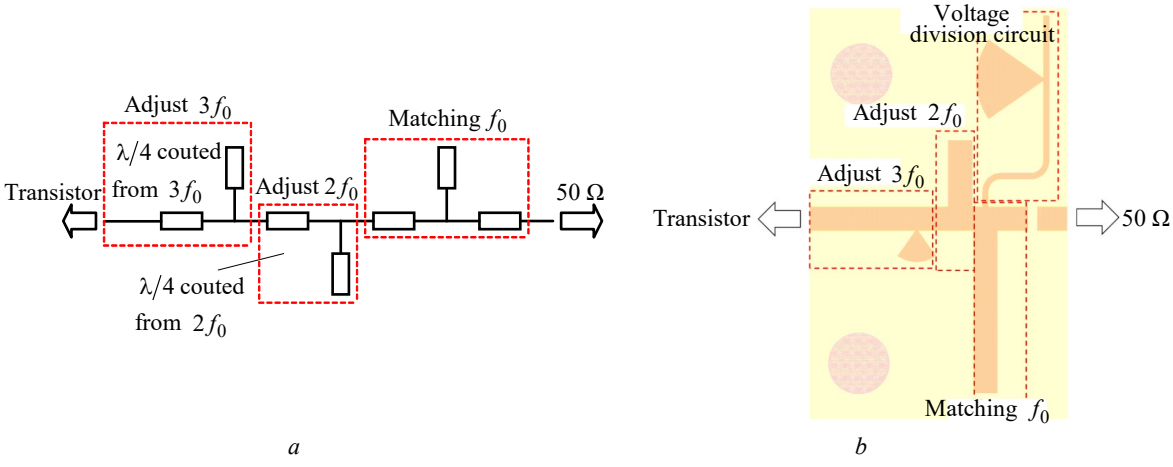

Fig. 9. Strip circuit of the output impedance matching at the ideal level (*a*) and layout circuit (*b*)

The output impedance matching circuit is designed similarly to the input impedance matching circuit, which is responsible for transmitting a signal from a source with an impedance of $Z_{L,f_0} \sim (9.6 - j4.1)\,\Omega$ (which is the optimal load impedance of the input impedance matching circuit of the PA element) to a load with an impedance of 50 Ω at the frequency $f = f_0 = 9.4$ GHz, while reducing the power loss at the 2nd and 3rd harmonics.

Fig. 9, *a* shows that there will be an open-circuit transmission line from the PA element side with the length $\lambda/4$ at frequencies $2f_0$ and $3f_0$ coupled in parallel with the main transmission line. The lengths of the main transmissions (series connection) can be adjusted such that, at the coupling points, a net reactance element will be formed to suppress the $2f_0$ and $3f_0$ harmonics. After that, one open-circuit transmission line and two serial lines will be used to perform power matching at the f_0 frequency.

Fig. 10 shows that the insertion loss characteristics of the output impedance matching circuit, depending on the frequency, demonstrate acceptably small values. At the f_0 frequency, the insertion loss IL has a value 0.42 dB, thus basically satisfying the design requirements.

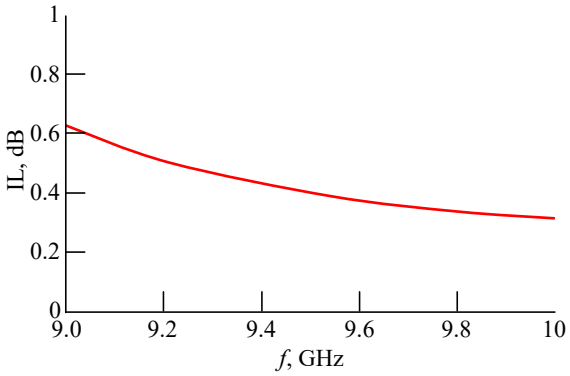

Fig. 10. Insertion loss characteristics of the output impedance matching circuit

Design of a voltage divider circuit.

1. Similarly to any radio electronic circuit, the voltage divider circuit of an PA performs the function of supplying DC power to establish the operating point of the active element and suppresses the RF signal to avoid loss and bad interference to a DC source.

2. According to [12], the voltage distribution for the circuits working in the X band, which was applied in this study, will use a conical open-circuit transmission and the $\lambda/4$ path segments as

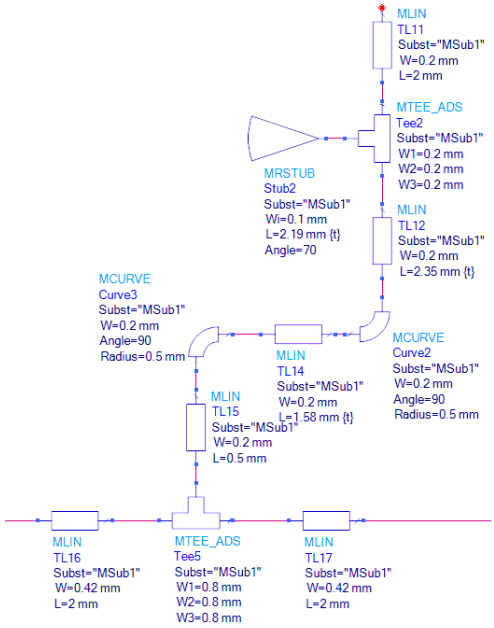

Fig. 11. Schematic diagram of the strip circuit of the voltage divider circuit

a short circuit capacitor (instead of pass capacitor) at the f_0 frequency as shown in Fig. 11.

The results of measuring and testing the quality of the voltage divider circuit through the parameters $S_{21} = -(0.061\ldots0.046)$ dB and $S_{11} \sim -50$ dB show its basic correspondence to the set requirements for an X-band PA.

3. The coupling capacitor used in the design has the code GJM0225C1C1R2BB01 with the parameters $C \sim (1.2 \pm 0.1)\,\text{pF}\big|_{f=10\text{ MHz}\ldots20\text{ GHz}}$, $S_{21} = -0.03\text{ dB}\big|_{f_0}$, $S_{11} \sim -43.7\text{ dB}\big|_{f_0}$ suitable for the design purposes.

Results of PA design and comments.

1. Fig. 12 presents a schematic of layout of the X band PA.

2. Fig. 13, *a*, *b* and *c* present the simulation results and experimental measurements $P_{\text{out}}\big|_{f=8.9\ldots9.8\text{ GHz}}$; $\text{PAE}\big|_{f=8.9\ldots9.8\text{ GHz}}$; and amplification factor (gain) $G_P\big|_{f=8.9\ldots9.8\text{ GHz}}$. On this basis, it becomes possible to evaluate the ability to stabilize the output power level, PAE, and gain of the designed PA when the working frequency of the signal changes in the required range.

3. In order to evaluate the capability of the designed PA to ensure linearity, we performed a direct test measure of the signal form at its output

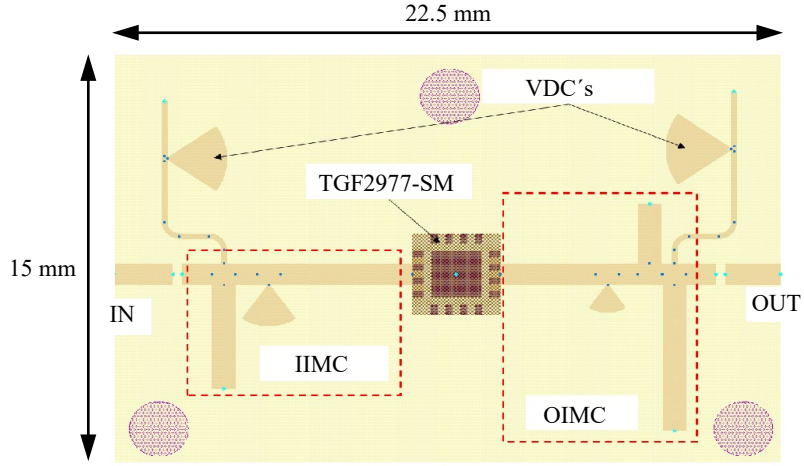

Fig. 12. Layout of the designed X band PA

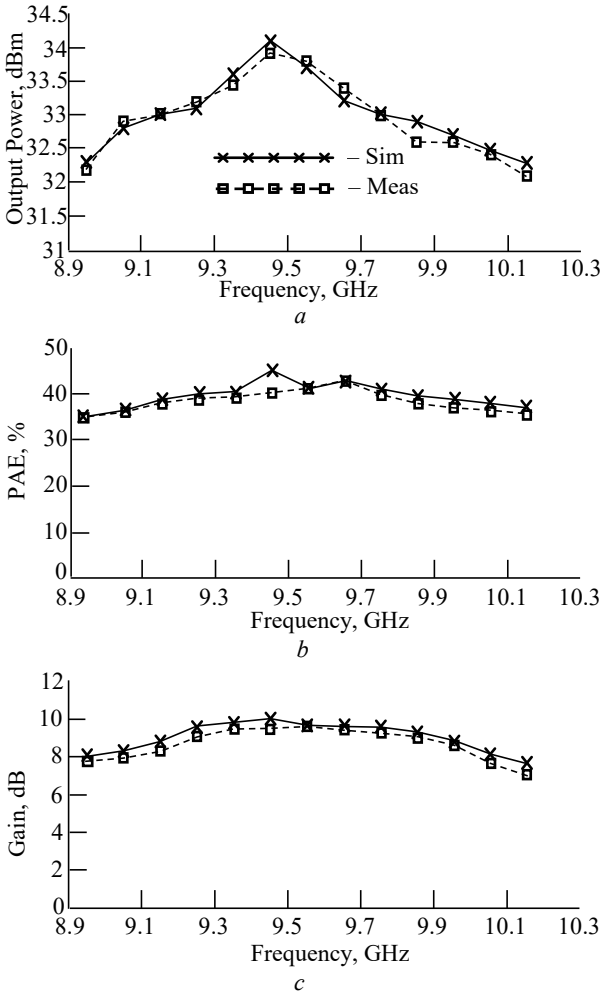

Fig. 13. Simulation results and experimental measurements of the $P_{\text{out}}\big|_{f=8.9\ldots9.8\,\text{GHz}}$ (*a*), $\text{PAE}\big|_{f=8.9\ldots9.8\,\text{GHz}}$ (*b*) and amplification factor (gain) $G_P\big|_{f=8.9\ldots9.8\,\text{GHz}}$ (*c*)

under the load of 50 Ω. In this respect, our work differs from other research studies.

Fig. 14 shows the results of the voltage and current signal waveforms on the drain of the PA

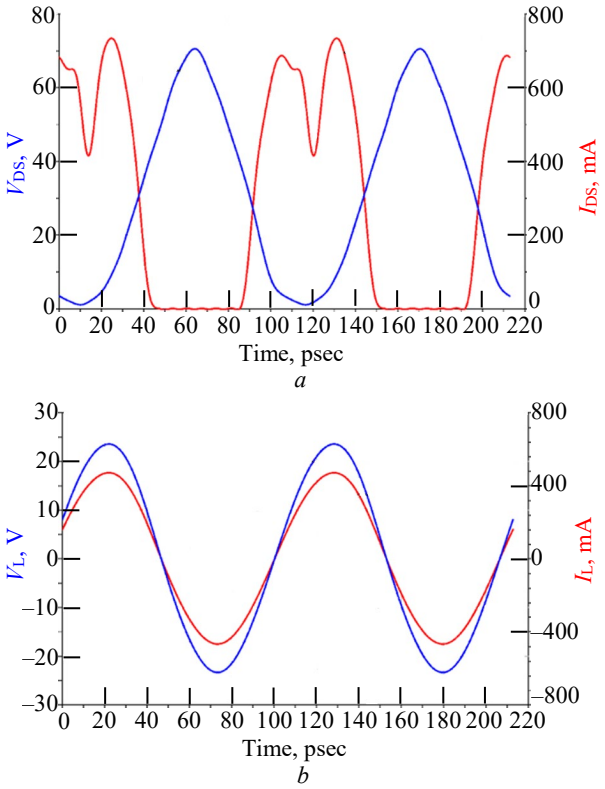

Fig. 14. Voltage and current signal waveforms on the drain of the PA element (*a*) and on the PA load (*b*)

element and under the load. It can be seen that the current and voltage on the PA element are out of phase, while they are in phase under the load. The current and voltage across the PA element are distorted due to the presence of harmonic components, where the current is cut to the form of a pulse in the AB mod with a flux angle greater than 90°. The current and voltage across the load, on the other hand, have an almost complete sinusoidal form, indicating an effective elimination of harmonics by means of harmonic compression using

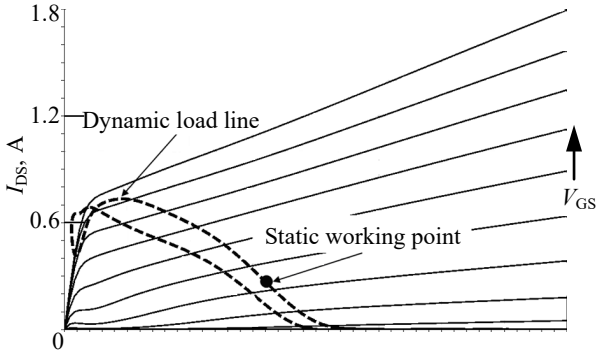

Fig. 15. Operating mode and working point described on the output characteristic

the approach described when designing and calibrating the in/out impedance matching circuits.

4. The operating mode and working point are described as the output characteristic of the PA element shown in Fig. 15. Accordingly, the current is swept to the maximum value $(700\,\text{mA})$. The variation of the current is shown on the dynamic load line. The linear range of voltage across the load is within the range of $-14.5\ldots+14.5$ V.

Tab. 4 presents the basic characteristics of the designed X-band UHF PA unit.

A comparison of the obtained PA characteristics with those presented in Table 1 shows that the designed X-band PA unit meets all the input requirements.

Tab. 4. The basic characteristics of the designed UHF PA X-band

№	Characteristics	Value
1	Frequency band, GHz	X
2	Range, GHz	8.9…9.8
3	f_0, GHz	9.4
4	P_{out}, dBm	32…33
5	PAE, %	35…40
6	GP, dB	8.5…10
7	2nd harmonic compression, dB	–32.5
8	3rd harmonic	–38.5

Conclusions. 1. The results of a study into the design of UHF power amplifiers working in the X band are presented. The authors' intention was not to propose a new design approach, but rather to clarify a method that combines theoretical calculations, experimental measurements, and experimental adjustments. This approach allowed the authors to harmonize and ensure optimization of some relationships between the basic characteristics of the amplifier, including frequency bandwidth, output power, output power variation, high harmonic suppression, and output signal linearity. The described implementation has practical significance in terms of simplicity and convergence between theory and experiment.

2. The results obtained can be used to develop a technological process and procedure for manufacturing X-band UHF PAs even under unfavorable technological and economic conditions.

3. The developed X-band UHF amplifier may find application in multifunctional electronic radio systems, such as communication, radio navigation, etc.

Author's contribution

Xuan Luong Nguyen, synthesis and analysis of approaches to solving engineering design problems and PA technology; theoretical analysis and selection of PA elements meeting the set technical requirements; drawing structural and functional diagrams; selection of options for a schematic diagram corresponding to the amplification modes.

Thanh Thuy Dang Thi, scientific advisor and scientific support, including simulation models for PA and PA elements by common ultra-high frequency design tools; analysis of the obtained results; supporting implementation using the Keysight ADS high frequency circuit simulation tool.

Van Bac Nguyen, scientific, technical, and technological support, including the implementation of PA design and technology using high frequency material RO4003C; participation in the process of measuring and correcting technical characteristics; supporting measurement and adjustment of technical specifications.

Phung Bao Nguyen, scientific advisor, consulting and controlling the entire process, including simulation, design, and manufacturing; measuring, calibrating and processing the data on the PA technical characteristics.

References

1. Wulf-Dieter Wirth. Radar Techniques Using Array Antennas. 2nd Ed.. London, The Institution of Engineering and Technology, 2013, 460 p.

2. Cripps S. C. RF Power Amplifiers for Wireless Communications. 2nd Ed. Norwood, Artech House, 2006, 474 p.

3. Wang J., He S., You F., Shi W., Peng J., Li Ch. Codesign of High-Efficiency Power Amplifier and Ring-Resonator Filter Based on a Series of Continuous Modes and Even-Odd-Mode Analysis. IEEE Trans. Microw. Theory Techn. 2018, vol. 66, iss. 6, pp. 2867–2878. doi: 10.1109/TMTT.2018.2819650

4. Thian M., Barakat A., Fusco V. High-Efficiency Harmonic-Peaking Class-EF Power Amplifiers with Enhanced Maximum Operating Frequency. IEEE Trans. Microw. Theory Techn. 2015, vol. 63, iss. 2, pp. 659–671. doi: 10.1109/TMTT. 2014.2386327

5. Poluri N., De Souza M. M. High-Efficiency Modes Contiguous with Class B/J and Continuous Class F^{-1} Amplifiers. IEEE Microw. Wireless Compon. Lett. 2019, vol. 29, iss. 2, pp. 137–139. doi: 10.1109/LMWC. 2018.2886655

6. García J. A., Popović Z. Class-E Rectifiers and Power Converters. 2017 IEEE MTT-S Intern. Microwave Symp. (IMS), Honololu, HI, 2017, pp. 1327–1330. doi: 10.1109/MWSYM.2017.8058856

7. Saxena S., Rawat K., Roblin P. Continuous Class-B/J Power Amplifier Using a Nonlinear Embedding Technique. IEEE Trans. Circuits Syst. II, Exp. Briefs. 2017, vol. 64, iss. 7, pp. 837–841. doi: 10.1109/TCSII.2016.2633300

8. Zhang Z., Cheng Z., Liu G. Design of Broadband Class EF Power Amplifier Based on Low-Pass Filter Matching Structure. IEICE Electronics Express. 2019, vol. 16, iss. 12, p. 20190264. doi: 10.1587/elex.16.20190264

9. Meng X., Yu C., Liu Y., Wu Y. Design Approach for Implementation of Class-J Broadband Power Amplifiers Using Synthesized Band-Pass and Low-Pass Matching Topology. IEEE Transactions on Microwave Theory and Techniques. 2017, vol. 65, iss. 12, pp. 4984–4996. doi: 10.1109/TMTT.2017.2711021

10. Shwetal P., Sunil K. Methods and Steps Required for the Development of a RF Power Amplifier. IJCRT. 2018, vol. 6, iss. 1, pp. 1742–1746.

11. Weiss M., Raab F., Popovic Z. Linearity of X-Band Class-F Power Amplifiers in High-Efficiency Transmitters. IEEE Transactions on Microwave Theory and Techniques. 2001, vol. 49, no. 6, pp. 1174–1179. doi: 10.1109/22.925515

12. Dong-Hwan Shin, In-Bok Yom, Dong-Wook Kim. X-Band GaN MMIC Power Amplifier for the SSPA of a SAR System. 2017 IEEE Intern. Symp. on Radio-Frequency Integration Technology (RFIT). Seoul, Korea (South), 30 August – 01 September 2017. IEEE, 2017. doi: 10.1109/RFIT.2017.8048093

13. Tran P., Smith M., Callejo L., Wojtowicz M., Siddiqui M. 2 to 18 GHz High-Power and High-Efficiency Amplifiers. 2017 IEEE MTT-S Intern. Microwave Symp. (IMS). Honololu, USA, 04–09 June 2017. IEEE, 2017. doi: 10.1109/MWSYM.2017.8058837

14. Kyung-Tae Bae, Ik-Joon Lee, Byungjoo Kang, Sanghoon Sim, Laurence Jeon, Dong-Wook Kim. X-Band GaN Power Amplifier MMIC with a Third Harmonic-Tuned Circuit. Electronics. 2017, vol. 6, iss. 4, p. 103. doi: 10.3390/electronics6040103

15. Ken Hiraga, Takashi Hikage, Manabu Yamamoto, Toshio Nojima. Harmonic Matchinh and Reflecting PA with 2nd and 3rd Harmonic Phase Tuning. 2012 Intern. Symp. on Antennas and Propagation (ISAP). Nagoya, Japan, October – 02 November 2012. IEEE, 2012.

16. Mjakin'kov V. Ju., Gubarev V. F., Rudyj Ju. B., Kovtunov D. A., Kalinin A. S., Fut'janov S. I., Rabodzej A. N., Shipilo E. M. *Priemoperedajushhij modul' doplerovskogo izmeritelja skorosti, ugla snosa i vysoty dlja sovremennyh samoletov* [Transmitter and Transmission Module for Doppler Velocity, Drift Angle and Altitude for Modern Aircraft]. Electronic Engineering, Ser. 1, Microwave Technology. 2013, no. 3(518), pp. 200–205.

17. Power Amplifiers. Available at: https://www.qorvo.com/products/amplifiers/power-amplifiers (accessed 05.11.2022)

18. TGF2977-SM. Available at: https://www.qorvo.com/products/d/da004922 (accessed 05.11.2022)

19. ADS 2016 Product Release. Available at: https://www.keysight.com/us/en/lib/resources/software-releases/ads-2016.html (accessed 05.11.2022)

20. PathWave Advanced Design System (ADS). Available at: https://www.keysight.com/us/en/lib/softwaredetail/computer-software/pathwave-advanced-design-system-ads-software-2212036.html (accessed 05.11.2022)

Information about the authors

Xuan Luong Nguyen, Master Degree (2013) in radio navigation systems at Le Quy Don Technical University, Vietnam. Systems Engineer at the Research Institute of Radio Navigation Systems. PhD student in at the Department of Radio Physics, VNU University of Science. The author of 1 scientific publications. Area of expertise: ultra-high frequency radio engineering; systems engineering of multifunctional systems
Address: VNU University of Science, 334, Nguyen Trai, Hanoi, Vietnam
E-mail: xuanluongfpga@gmail.com

Dang Thi Thanh Thuy, PhD (2012), lecturer at the Department of Radio Physics, VNU University of Science. Associate Professor (2018). The author of 30 scientific publications. Area of expertise: ultra-high frequency techniques; parameter oscillation; ultrasound techniques.
Address: VNU University of Science, 334, Nguyen Trai, Hanoi, Vietnam
E-mail: dangthithanhthuy@vnu.edu.vn

Phung Bao Nguyen, PhD (1996), Visiting Lecturer of the Institute of System Integration/TU Le Quy Don; Former Director of the Institute of System Integration/TU Le Quy Don; Former Deputy of Director of the IMC/VUSTA/Ministry of Science & Technology/SRV. The author of 26 scientific publications. Area of expertise: radar information processing; radioelectronic and radar technology; systems engineering.
Address: Le Quy Don Technical University, 236, Hoang Quoc Viet, Hanoi, Vietnam
E-mail: nguyenphungbao@lqdtu.edu.vn; baonp@imc.org.vn

Van Bac Nguyen, Master Degree (2013) in Radar Engineering of Military Academy of Field Anti-Aircraft Defense named after Marshal of Soviet Union A. M. Vasilevsky, Russian Federation. Lecturer of the Department of Electronic Technologies of Institute of System Integration/TU Le Quy Don. The author of 6 scientific publications. Area of expertise: radar and radio navigation; telecommunications.
Address: Le Quy Don Technical University, 236, Hoang Quoc Viet, Hanoi, Vietnam
E-mail: nvback42@gmail.com